

A Swap-Adversarial Framework for Improving Domain Generalization in Electroencephalography-Based Parkinson’s Disease Prediction

Seongwon Jin^a, Hanseul Choi^a, Sunggu Yang^{b,c}, Sungho Park^{a,*}, Jibum Kim^{a,c,*}

^a*Department of Computer Science and Engineering, Incheon National University, Yeonsu-gu, 22012, Incheon, Republic of Korea*

^b*Department of Nanobioengineering, Incheon National University, Yeonsu-gu, 22012, Incheon, Republic of Korea*

^c*Center for Brain-Machine Interface, Incheon National University, Yeonsu-gu, 22012, Incheon, Republic of Korea*

Abstract

Electroencephalography (ECoG) offers a promising alternative to conventional electrocorticography (EEG) for the early prediction of Parkinson’s disease (PD), providing higher spatial resolution and a broader frequency range. However, reproducible comparisons has been limited by ethical constraints in human studies and the lack of open benchmark datasets. To address this gap, we introduce a new dataset, the first reproducible benchmark for PD prediction. It is constructed from long-term ECoG recordings of 6-hydroxydopamine (6-OHDA)-induced rat models and annotated with neural responses measured before and after electrical stimulation. In addition, we propose a Swap-Adversarial Framework (SAF) that mitigates high inter-subject variability and the high-dimensional low-sample-size (HDLSS) problem in ECoG data, while achieving robust domain generalization across ECoG and EEG-based Brain-Computer Interface (BCI) datasets. The framework integrates (1) robust preprocessing, (2) Inter-Subject Balanced Channel

*Corresponding to: Department of Computer Science and Engineering, Incheon National University, Yeonsu-gu, 22012, Incheon, Republic of Korea

Email addresses: jinwork00@gmail.com (Seongwon Jin), himlm0704@gmail.com (Hanseul Choi), sungguyang@inu.ac.kr (Sunggu Yang), yunisomi@inu.ac.kr (Sungho Park), jibumkim@inu.ac.kr (Jibum Kim)

Swap (ISBCS) for cross-subject augmentation, and (3) domain-adversarial training to suppress subject-specific bias. ISBCS randomly swaps channels between subjects to reduce inter-subject variability, and domain-adversarial training jointly encourages the model to learn task-relevant shared features. We validated the effectiveness of the proposed method through extensive experiments under cross-subject, cross-session, and cross-dataset settings. Our method consistently outperformed all baselines across all settings, showing the most significant improvements in highly variable environments. Furthermore, the proposed method achieved superior cross-dataset performance between public EEG benchmarks, demonstrating strong generalization capability not only within ECoG but to EEG data. The new dataset and source code will be made publicly available upon publication.

Keywords: Brain–Computer Interface (BCI), Electrocorticography (ECoG), Electroencephalography (EEG), Parkinson’s Disease Prediction, Domain Generalization, Classification

1. Introduction

Parkinson’s disease (PD) is a progressive neurodegenerative movement disorder caused by the selective loss of dopaminergic neurons in the substantia nigra pars compacta, leading to bradykinesia, rigidity, tremor, and postural instability (Kalia and Lang, 2015). While the global aging population leads to a steady increase in the number of patients with PD and the resulting social and economic burden, early detection and treatment remain challenging since clinical diagnosis is generally possible after the onset of visible motor symptoms (Obeso et al., 2017; Dorsey et al., 2018). Nonetheless, several studies have been conducted to alleviate motor symptoms in patients with PD by placing electrodes in specific regions of the brain and applying electrical stimulation. For instance, some studies have shown that continuous electrical stimulation can reduce tremor and rigidity in PD patients (Benabid et al., 2009; Weaver et al., 2009), and others have explored approaches to modulate stimulation in real time by sensing brain activity (Little et al., 2013). However, they are limited to patients whose symptoms have already become apparent. Therefore, recent studies have focused on combining brain signals (*e.g.*, EEG and ECoG) with deep learning models to enable the early diagnosis of PD. (Abumaloh et al., 2024; Neves et al., 2024).

Among various brain recording modalities, Electroencephalography (EEG)

is a non-invasive technique that captures brain electrical activity through scalp electrodes. Due to its simple setup and suitability for repeated measurements, EEG has been the most widely used modality in deep learning-based studies for PD prediction (Oh et al., 2020). However, as the signals pass through the skull, scalp, and cerebrospinal fluid, their high-frequency components are severely attenuated, and spatial resolution is reduced to about the centimeter level. This makes it difficult to accurately capture the characteristic patterns of PD, such as local fluctuations in β -band activity and pathological high-frequency oscillations (HFOs) (Srinivasan et al., 2007). Therefore, electrocorticography (ECoG), which directly measures signals from the cortical surface beneath the skull with millimeter-level spatial resolution and stable access to high-frequency bands, has emerged as a promising modality for predicting PD. (Lachaux et al., 2012; Ali et al., 2022; Kim et al., 2025). Due to its high signal-to-noise ratio (SNR) and wide frequency bandwidth, ECoG allows deep learning models to more accurately capture complex neurophysiological patterns.

However, invasive ECoG studies involving human subjects are limited by ethical and safety concerns. As a result, many prior studies have collected ECoG data for experimental analysis from animal models of PD induced by 6-hydroxydopamine (6-OHDA) and from control animals (Kim et al., 2025; Shin et al., 2025; Wang et al., 2024a). In addition, a previous study (Wang et al., 2024a) released a publicly available dataset collected from 6-OHDA-induced rats for closed-loop deep brain stimulation (DBS) and biomarker analysis. However, the ECoG channels used for recording in this dataset are inconsistent across subjects and their different states, making it difficult to train deep learning models and perform reliable comparative experiments. Accordingly, we constructed a new dataset by assigning labels corresponding to the disease states before and after electrical stimulation, based on the long-term ECoG recordings from 11 6-OHDA-lesioned rats proposed in (Shin et al., 2025). Furthermore, we organized this dataset into a data partitioning and cross-validation framework for unseen-domain evaluation, establishing the first ECoG-based benchmark for PD prediction, named MOCOP, which can be used for both training and evaluation of deep learning models.

On the other hand, because ECoG electrodes are directly implanted on the cortical surface, the recorded signal characteristics can exhibit substantial inter-subject variability due to anatomical factors such as electrode placement and cortical folding structure (Miller et al., 2010). Moreover, during long-term recordings that may span from several days to even months, the

degree of temporal non-stationarity tends to increase considerably, leading to much greater inter-subject variability compared to EEG signals (Ung et al., 2017). Such high variability often leads to subject dependency, where the model overfits to the feature distribution of specific subjects in the training set, resulting in a significant degradation in inference performance on unseen subjects (Ali et al., 2022).

To mitigate this issue, previous studies have proposed domain adaptation and domain generalization approaches to learn invariant representations from EEG and ECoG data, aiming to achieve robustness against inter-subject variability (Ma et al., 2019; Melbaum et al., 2022; Chen et al., 2025). In particular, one of the most widely adopted approaches is domain adversarial learning, which jointly trains a feature encoder and a domain discriminator in an adversarial manner to effectively eliminate domain-specific characteristics across diverse tasks (Ganin et al., 2016; Kamnitsas et al., 2016; Woo et al., 2024). Compared with methods that minimize the performance gap of the worst group (Sagawa et al., 2019) or reduce feature distribution discrepancies in lower-level or intermediate feature spaces (Reddi et al., 2015; Cheng and Xie, 2024), domain adversarial learning is more effective for learning robust representations against inter-subject variability by directly eliminating subject-specific information in high-dimensional feature spaces (Ma et al., 2019). Although domain adversarial learning has been explored in EEG-based BCI studies, its application to ECoG data has remained relatively limited. In this work, we present the first application of domain adversarial learning for domain generalization in an ECoG-based PD prediction model, aiming to learn subject-independent representations and enhance the generalization capability of the model on unseen subjects.

However, ECoG data typically exhibit a high-dimensional and low-sample-size (HDLSS) property due to the limited number of subjects and the high cost of data collection, which often leads to unstable model convergence and overfitting during adversarial training (Śliwowski et al., 2023). Furthermore, ECoG electrode configurations and cortical structures vary substantially across subjects. These anatomical differences directly affect the target task, inducing a strong correlation between subject-dependent characteristics and task-relevant information (Haufe et al., 2018; Memar et al., 2025). As a result, directly applying conventional domain adversarial approaches can even degrade performance, as task-relevant information can be unintentionally removed along with subject-specific features (Dayanik and Padó, 2021).

To address these challenges, we propose a data augmentation method

called Inter-Subject Balanced Channel Swap (ISBCS) that accounts for the intrinsic characteristics of ECoG signals. The method randomly swaps corresponding channels across subjects to generate counterfactual samples, thereby increasing the diversity of data distributions and alleviating structural biases among subjects. It encourages the encoder to learn task-relevant and subject-invariant representations rather than subject-specific features. This allows the subsequent domain adversarial learning to remove the already weakened subject dependency with minimal loss of task-relevant information, thereby improving training stability and cross-subject generalization performance.

Building on this, we present a novel learning framework, called the Swap-Adversarial Framework, which consists of three complementary components: preprocessing, data augmentation, and domain adversarial learning. In the first component (i.e., preprocessing), various types of noise in ECoG signals are refined to minimize distortion in the latent feature distribution. Specifically, the Artifact Subspace Reconstruction (ASR) method (Mullen et al., 2015) is utilized to remove high-amplitude, low-dimensional artifacts, thereby suppressing the high-energy noise frequently observed in ECoG recordings. This process not only enables the feature encoder to reliably learn meaningful neurophysiological patterns but also prevents the domain discriminator in the subsequent adversarial learning stage from focusing on irrelevant high-energy components, which could hinder effective bias removal. Subsequently, in the data augmentation process, corresponding channels are randomly swapped across subjects to generate counterfactual samples. This increases the diversity of data distributions and weakens subject-specific structural cues, encouraging the model to focus on task-relevant features. Finally, during domain adversarial learning, the encoder and task-specific classifier are jointly optimized for the target task, while the encoder and domain discriminator are adversarially trained to further suppress any remaining subject-specific features. This process preserves task-relevant information while minimizing subject-dependent bias, thereby improving cross-subject generalization performance.

In the experimental section, we extensively validated the effectiveness of the proposed method from multiple perspectives. First, in cross-subject experiments using ECoG datasets, the proposed framework outperformed all baselines, demonstrating its superior performance. In addition, in domain generalization experiments across different signal acquisition environments (*i.e.*, wireless and wired), the proposed method showed robust performance under variations in equipment and acquisition conditions. Finally, in cross-

dataset evaluations between public EEG benchmarks, the proposed method was effectively applied to the EEG domain and mitigated dataset-level domain gaps, demonstrating strong generalization capability across modalities.

Our main contributions are summarized as follows.

1. We constructed and publicly released a benchmark dataset, MOCOP, which includes ECoG recordings and corresponding state labels obtained from experimental rats with PD induced by 6-Hydroxydopamine (6-OHDA) lesions. The dataset will be made publicly available upon publication.
2. We propose a novel learning framework to learn domain-invariant representations based on brain signal modalities (e.g., ECoG and EEG). It generates counterfactual samples by randomly swapping corresponding channels between subjects, thereby preventing the encoder from learning subject-dependent features. Subsequently, domain adversarial learning is applied to remove the remaining subject-dependent features, thereby enhancing generalization performance while preserving task-relevant information.
3. Through extensive experiments, we demonstrate that the proposed framework significantly outperforms all baselines in both cross-subject and cross-environment settings. Furthermore, it achieves superior cross-dataset performance on public EEG benchmarks, showing the scalability and general applicability of the proposed framework to various electrophysiological signal modalities.

2. Related work

2.1. Early Prediction of Parkinson’s Disease

Agrawal and Sahu (2025) and Jeong et al. (2016) investigated Parkinson’s disease (PD) diagnosis using statistical approaches such as spectral and wavelet-based analyses. However, these statistical methods are limited in quantifying the complex brain dynamics underlying PD. In particular, they fail to capture the nonlinear patterns and subject-specific characteristics inherent in brain signals (Obayya et al., 2023; Schlogl et al., 1996). To overcome these limitations, recent studies have introduced deep learning-based methods for brain signal analysis. Oh et al. (2020) first proposed a deep learning-based approach for PD diagnosis using EEG. They designed a CNN model that classified normal and PD subjects directly from EEG

inputs, demonstrating the potential of deep learning for PD prediction. In addition, Shah et al. (2020) proposed DGHNet, a hybrid model combining CNN and LSTM architectures, achieving efficient performance with fewer parameters in classifying PD and healthy subjects from EEG signals. However, this model relied heavily on subject-specific characteristics, leading to poor inter-subject generalization.

2.2. ECoG-based Prediction

Although research using ECoG signals has been limited due to the difficulty of data acquisition, recent studies have increasingly explored deep learning-based prediction with ECoG. Ji (2024) proposed a deep learning model that classified visual stimuli viewed by monkeys based on ECoG recordings. In experiments with two monkeys, the proposed model achieved relatively high accuracy in within-subject evaluations but dropped to approximately 16% in cross-subject evaluations, indicating that ECoG signals exhibit substantial inter-subject variability. In addition, ECoG signals have also been utilized for seizure classification. Lam et al. (2024) proposed a model leveraging self-supervised learning to effectively classify seizures with limited data. Their approach involved masking parts of the input spectrogram and training the model to reconstruct the missing regions, thereby enabling it to learn key signal representations. Furthermore, a study has also addressed the performance degradation caused by inter-subject distributional differences in ECoG signals from epilepsy patients. Cui et al. (2022) proposed a framework that minimizes the joint distribution discrepancy between source and target domains, while leveraging target-domain clustering to align source class centroids with cluster prototypes. In cross-subject evaluations, this framework outperformed conventional domain adaptation methods, demonstrating its effectiveness in mitigating inter-subject variability. Moreover, Bore et al. (2020) proposed a classification model that distinguishes Parkinsonian states from healthy controls based on ECoG data. Using SVM-RBF and KNN classifiers, the model achieved a high prediction accuracy of approximately 98%, but its generalization to other subjects was not validated.

2.3. General Approaches to Domain Generalization

Domain generalization aims to train models that maintain robust performance on unseen target domains without accessing target-domain data during training. This technique has been extensively studied across a wide range of fields (Ganin et al., 2016; Li et al., 2018; Dayal et al., 2023; Shankar

et al., 2018; Muandet et al., 2013). One of the primary approaches to domain generalization is to learn domain-invariant features. To achieve this, several studies on domain-adversarial learning (Ganin et al., 2016; Yang et al., 2020; Li et al., 2018) train a feature encoder and a domain classifier in an adversarial manner, encouraging the encoder not to learn domain-specific representations. Another line of work (Bore et al., 2020; Dayal et al., 2023) adopts MMD-based strategies to explicitly minimize feature distribution discrepancies across domains, leading to more domain-invariant representations. Furthermore, Arjovsky et al. (2020) introduced Invariant Risk Minimization (IRM), which aims to learn the relationships between invariant features and labels across multiple domains. In a different line of work, Sagawa et al. (2019) proposed Group Distributionally Robust Optimization (Group DRO) which trains the model to minimize the worst-group loss within the training distribution, thereby improving robustness under distribution shifts.

In this study, the subject dependency in ECoG data mainly arises from substantial variability in high-dimensional feature distributions across subjects. Therefore, instead of adopting distribution alignment methods (Bore et al., 2020; Dayal et al., 2023), which are suitable for reducing lower-level or intermediate feature distribution discrepancies, or worst-group optimization approaches (Sagawa et al., 2019) designed to improve performance for under-represented groups, we employ a domain-adversarial learning strategy that explicitly removes subject-specific information to extract subject-invariant representations.

2.4. Domain Generalization in EEG Analysis

Domain generalization approaches have been actively applied in the field of EEG signal analysis. Ma et al. (2019) proposed DG-DANN, an extension of the conventional Domain-Adversarial Neural Network (DANN) (Ganin et al., 2016) into the domain generalization setting, along with a corresponding DResNet model for EEG-based emotion classification tasks. The proposed method achieved high performance under the leave-multiple-random-subjects-out evaluation, demonstrating that domain generalization techniques can be effectively applied to EEG-based emotion classification tasks. In addition, Wang et al. (2024b) proposed DMMR, a domain generalization framework that extends the Mixup method by generating augmented feature representations through the mixing of data from different subjects in the latent space. Furthermore, Tao et al. (2024) proposed a method called Local Domain Generalization with a low-rank constraint (LDG), which enhances

domain generalization by modeling fine-grained correlations between subdomains in the source domain and the target domain. However, to the best of our knowledge, domain generalization approaches have not yet been applied to ECoG analysis. This is mainly due to the difficulty of data collection and the limited availability of ECoG datasets, which make it challenging to train and evaluate models across subjects. In this study, we propose the first domain generalization framework primarily designed for ECoG, which mitigates inter-subject variability inherent in ECoG signals.

3. Method

The overall architecture of the proposed Swap-Adversarial Framework is illustrated in Figure 1. The framework consists of three main stages. First, a preprocessing stage enhances signal fidelity by removing various types of noise from the ECoG recordings. Second, the counterfactual data augmentation stage alleviates structural domain discrepancies caused by inter-subject variability by randomly swapping corresponding channels across subjects. Finally, the domain adversarial learning stage trains the encoder and domain discriminator adversarially to suppress subject-specific features and learn domain-invariant representations.

3.1. Preliminary

3.1.1. Problem formulation

We consider a binary classification problem with two labels. In this setting, we use data collected from L individual subjects, denoted as $1, 2, \dots, L$. For each subject j , the dataset is represented as $D_j = (x_i^{(j)}, y_i^{(j)}, s_i^{(j)})_{i=1}^{n_j}$, where $x_i^{(j)} \in \mathbb{R}^{C \times M}$ denotes the i -th ECoG/EEG sample from subject j , $y_i^{(j)}$ is its class label (*e.g.*, pre-stimulation (Parkinsonian) or post-stimulation (functionally improved condition), and $s_i^{(j)}$ indicates the subject identity. Each sample $x_i^{(j)}$ consists of C channels and M temporal samples, representing a multichannel time series of neural activity. We divide the collected data into source domains D_S and target domains D_T . The source domains $D_S = D_1, D_2, \dots, D_K$ consist of K domains used for training, while the target domains correspond to unseen domains excluded from training. A feature extractor $f_\theta : \mathbb{R}^{C \times M} \rightarrow \mathbb{R}^d$ and a classifier $g_\phi : \mathbb{R}^d \rightarrow \mathbb{R}^2$ are trained solely on the source domains D_S . The objective is for the resulting model $g_\phi \circ f_\theta$ to accurately predict labels y for both the source and unseen target domains.

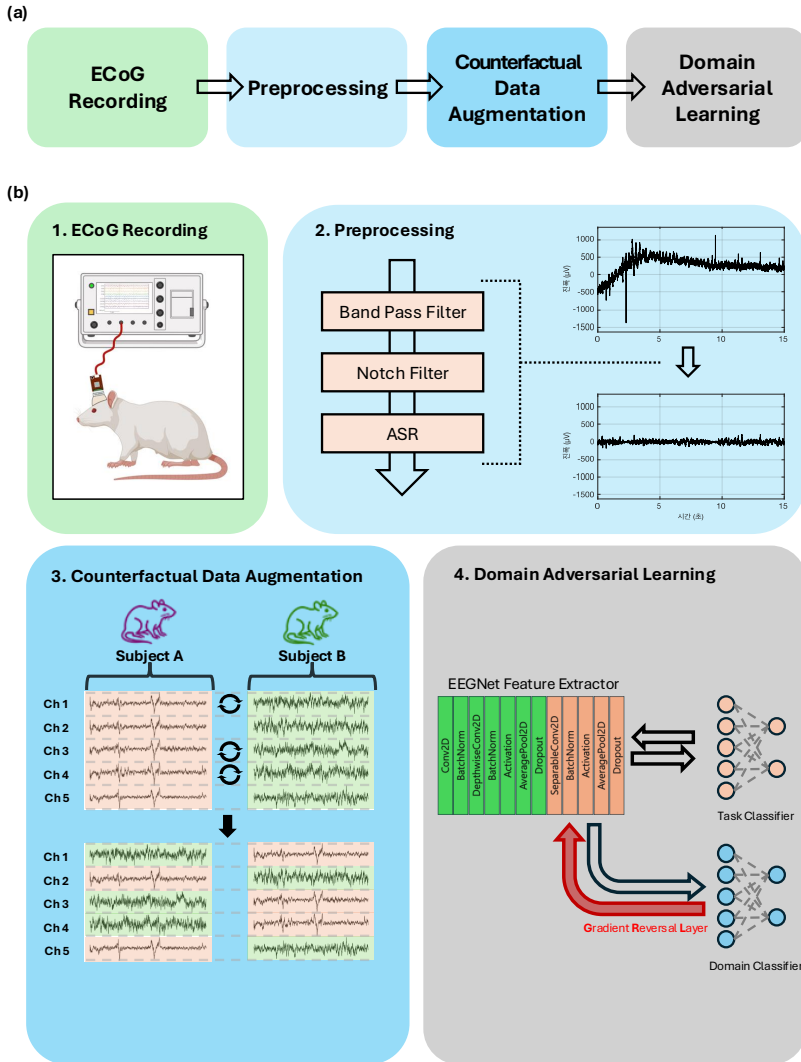


Figure 1: The overall architecture of Swap-Adversarial Framework. (a) The overall pipeline consists of four main stages: ECoG recording, preprocessing, counterfactual data augmentation, and domain adversarial learning. (b) Detailed illustration of each stage: (1) ECoG recording from subjects, (2) preprocessing including band-pass filtering, notch filtering, and ASR, (3) counterfactual data augmentation through Inter-Subject Balanced Channel Swapping (ISBCS) between Subject A and Subject B, (4) domain adversarial learning using EEGNet with task and domain classifiers.

3.1.2. Backbone Network

In this study, we adopt EEGNet (Lawhern et al., 2018) as the backbone model, which is a lightweight neural network widely used for brain-signal analysis (*e.g.*, EEG and ECoG). EEGNet achieves high performance with substantially fewer parameters compared to conventional CNN-based architectures. The model comprises a feature extractor f_θ , which consists of two main blocks, and a classifier g_ϕ (Cui et al., 2023). In the first block of the feature extractor, temporal convolution layers extract frequency-specific features from brain signals, followed by depthwise convolutions that learn spatial representations across channels. The second block applies separable convolutions, which combine depthwise and pointwise operations to model relationships among feature maps. The classifier g_ϕ , composed of a fully connected layer, predicts the target label y based on the feature representation z obtained from the feature extractor f_θ .

3.2. Pre-processing

ECoG signals provide superior spatial resolution, signal-to-noise ratio (SNR), and frequency bandwidth compared to EEG signals (Kanth and Ray, 2020). However, because ECoG is typically recorded over extended periods in freely moving subjects, the data often contain substantial noise, necessitating a preprocessing stage for noise reduction.

For noise removal in brain signals, various approaches such as Independent Component Analysis (ICA) (Makeig et al., 1995), Empirical Mode Decomposition (EMD) (Huang et al., 1998), and Variational Mode Decomposition (VMD) (Dragomiretskiy and Zosso, 2014) have been proposed. However, these methods often require direct expert intervention, which limits their practicality for large-scale or automated preprocessing. Therefore, we employed Artifact Subspace Reconstruction (ASR) (Mullen et al., 2015), an automated noise removal approach. It effectively eliminates high-energy, high-amplitude, and low-dimensional artifacts while preserving brain signals and handling non-repetitive artifacts (Chang et al., 2018). Therefore, this method is particularly suitable for the ECoG classification task, where unpredictable and diverse noise frequently occurs. In particular, it helps mitigate the issue in domain adversarial learning where the domain discriminator tends to focus on irrelevant high-energy noise, thereby hindering effective removal of subject-dependent features.

The proposed framework removes artifacts from brain signals through a sequential application of three filtering methods: a band-pass filter, a notch

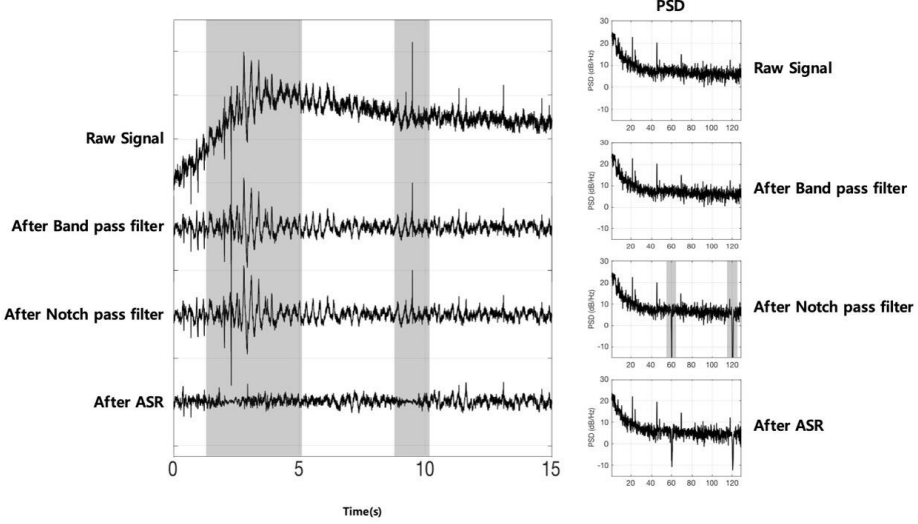


Figure 2: Visualization of the preprocessing pipeline. A representative 15-second segment demonstrating the signal changes during noise removal is presented. Noise removal is applied sequentially using a band-pass filter, a notch filter, and artifact subspace reconstruction (ASR).

filter, and artifact subspace reconstruction (ASR). The overall process can be expressed as follows:

$$\bar{x} = \text{Slicing}(\text{ASR}(\text{Notch}(\text{Bandpass}(x))))$$

All preprocessing steps are applied to the entire length of the ECoG recordings at once, after which the processed data are segmented according to a predefined window size. Descriptions of each method are provided below.

Band-pass filtering. A band-pass filter between 1 Hz and 128 Hz was applied to remove low-frequency noise associated with eye blinks and muscle movements, as well as high-frequency noise and detrending effects.

Notch filtering. To suppress power-line interference, notch filters at 60 Hz and its harmonic (*i.e.*, 120 Hz) were applied, selectively removing those specific frequency components.

ASR. To eliminate unpredictable and non-repetitive artifacts, ASR was applied. It detects clean calibration segments with low noise variance to estimate a reference subspace and removes components that exceed an RMS-based threshold, reconstructing the signal from the remaining components

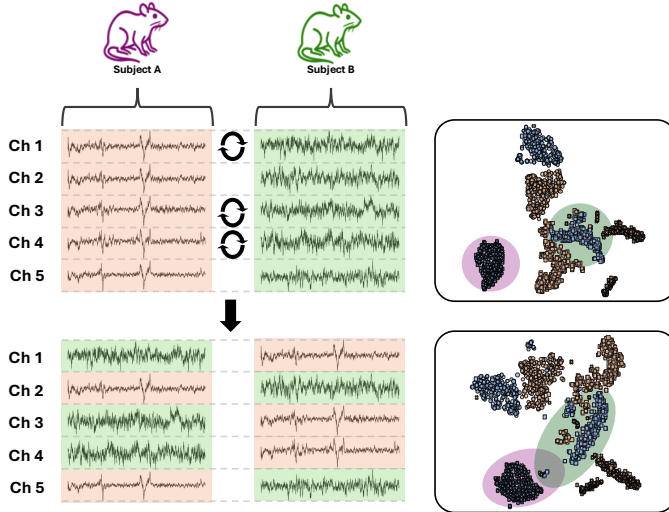


Figure 3: Inter-Subject Balanced Channel Swap (ISBCS): A counterfactual data augmentation method randomly swaps channel data between subject A and B with the same class. The t-SNE visualization shows that ISBCS induces overlapping distributions between subjects, reducing the inter-subject distributional separability. Here, the red and green circles represent different subjects, respectively.

(Chang et al., 2018).

As shown in Figure 2, we visualize the denoising process of a representative sample step by step in both the time and frequency domains. The band-pass filter removed low-frequency drifts and high-frequency noise, while the notch filter suppressed the 60 Hz and 120 Hz interference. Finally, ASR eliminated artifacts between 1–5 s and around 10 s.

3.3. Domain generalization

3.3.1. Counterfactual Data Augmentation

ECoG signals suffer from large inter-subject variability caused by individual biological differences, which hinders model generalization (Huang et al., 2023). To mitigate this structural bias and enhance model generalization, we propose a novel data augmentation method called Inter-Subject Balanced Channel Swap (ISBCS). Conventional data augmentation methods can improve classification performance and training stability by generating samples similar to the original data, but they are limited in reducing inter-subject

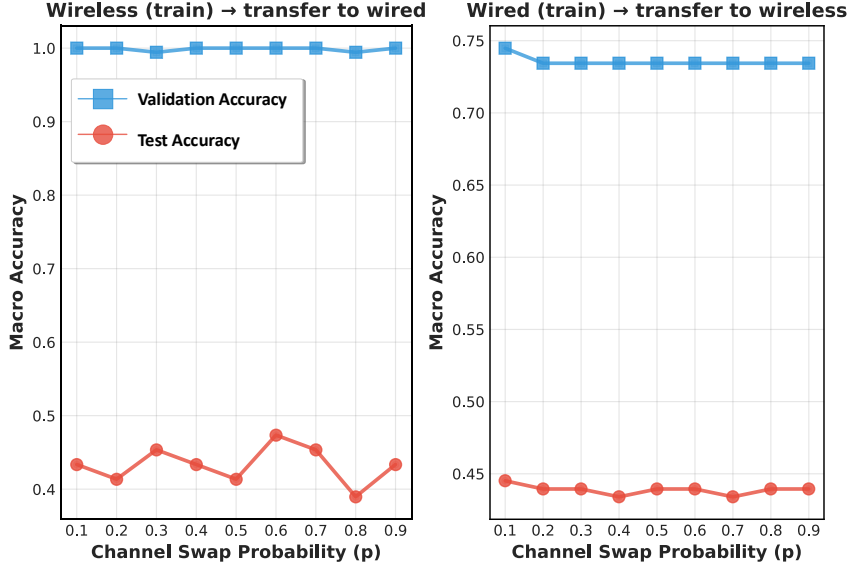


Figure 4: Sensitivity analysis of the ISBCS channel-swap probability p . (Left) Wireless (train) → transfer to wired (cross-subject); (Right) Wired (train) → transfer to wireless (cross-subject).

variability (Kamycki et al., 2020; Rommel et al., 2022).

In contrast, ISBCS randomly swaps corresponding channel data between samples from different subjects of the same class, encouraging the model to learn task-relevant and domain-invariant features rather than subject-specific features, as shown in Figure 3. Moreover, as shown in Figure 4, ISBCS is relatively insensitive to changes in the channel-swap probability p , making it simple to apply without extensive hyperparameter tuning.

Specifically, ISBCS first determines which channels to exchange by sampling from a Bernoulli distribution with probability p , where each channel is independently selected for swapping. Then, it randomly permutes the subject indices to define the pairing of subjects whose channel data will be exchanged. The swapping is performed only between samples belonging to the same class to maintain label consistency.

Finally, the augmented data are used to train the classification model as follows:

$$L_{task} = E_{(\bar{x}, y) \sim D'_S} L_{CE}(g_\phi(f_\theta(\bar{x})), y) \quad (1)$$

where $D'_S = (\bar{x}'_i, y_i, s_i)_{i=1}^N$ denotes the augmented dataset generated by the ISBCS method, and L_{CE} is the cross-entropy loss.

3.3.2. Domain Adversarial Learning

ISBCS mitigates subject-specific bias at the data level by swapping channels between samples from different subjects of the same class. We further introduce domain adversarial learning to suppress subject-dependent features, yielding domain-invariant representations and improved generalization to unseen domains.

To this end, we design the architecture for domain adversarial learning inspired by the approach of Kim et al. (2019). Specifically, a domain classifier (h_ψ) is employed to predict the subjects s from the feature representation z . First, the augmented data D' are fed into the feature extractor, which encodes them into the feature representation z . The features are then passed through a Gradient Reversal Layer (GRL) (Ganin et al., 2016), followed by the domain classifier. The GRL performs an identity mapping during the forward pass, but multiplies the gradient by a factor of $-\lambda_{GRL}$ during backpropagation, enabling adversarial learning between the feature extractor and the domain classifier. As a result, the domain classifier learns to predict the subject labels accurately, while the feature extractor learns to suppress subject-specific information, resulting in domain-invariant representations. The corresponding optimization objective is formulated as a minimax problem:

$$L_{domain} = \min_{\psi_h} \max_{\theta_f} E_{(\bar{x}, s) \sim D'_S} L_{CE}(h_\psi(f_\theta(\bar{x})), s) \quad (2)$$

In addition, we introduce a loss L_{MI} to suppress the mutual information between the feature vector z and the subject s , based on the probability distribution over subjects predicted by the domain classifier.

$$L_{MI} = E_{z \sim f_\theta(\bar{x})} H(h_\psi(z)), \text{ where } H(p) = - \sum_{i=1}^L p_i \log p_i \quad (3)$$

Finally, the overall objective is defined as follows:

$$L_{total} = L_{task} + \lambda_{MI} \cdot L_{MI} + \lambda_{GRL} \cdot L_{domain} \quad (4)$$

Here, λ_{MI} and λ_{GRL} are hyperparameters that control the relative importance of each loss term, leading the feature extractor to learn domain-invariant representations that generalize well to unseen domains.

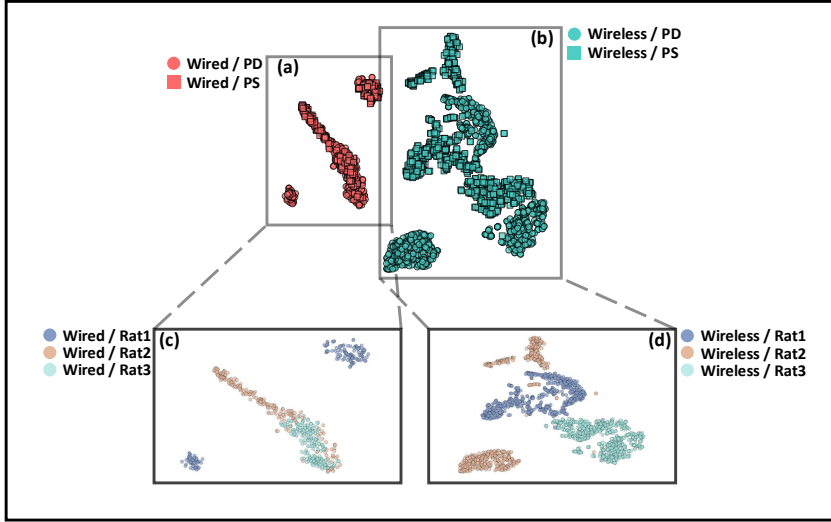


Figure 5: t-SNE visualization of the ECoG data after power spectral density (PSD) transformation. (a), (b) Distributions of all subjects in the wired and wireless datasets, respectively. (c) Distributions of individual subjects in the wired dataset. (d) Distributions of individual subjects in the wireless dataset. PS denotes the Post-Stimulation state, while PD denotes Parkinson’s Disease.

	Wireless			Wired		
	Rat 1	Rat 2	Rat 3	Rat 4	Rat 5	Rat 6
Class 0 (Parkinson’s disease)	301	308	304	78	99	108
Class 1 (Post-stimulation)	308	297	333	114	99	99

Table 1: Number of samples in the ECoG dataset.

4. Datasets

4.1. ECoG Dataset

4.1.1. Data Acquisition from Previous Study

To construct the training and evaluation datasets for the ECoG-based PD prediction model, we utilized the data collected in a previous study (Shin et al., 2025). Specifically, PD was induced in eleven healthy rats using the 6-OHDA method, and ECoG signals were recorded from seven of them. One subject with severe noise contamination was excluded, and the remaining six rats were used for the experiments.

Among the six rats, ECoG recordings were obtained from three rats using a wired system for 12 days and from the other three rats using a wireless

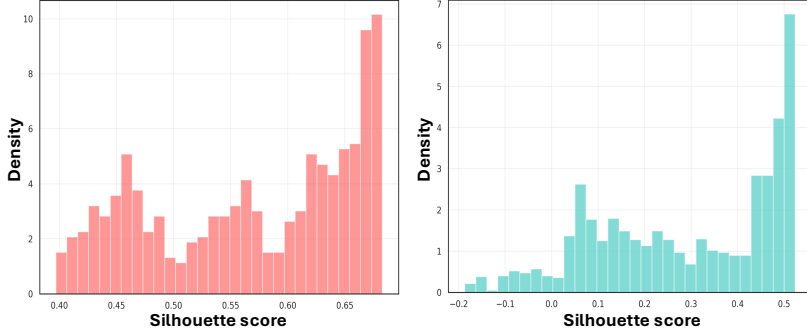


Figure 6: Silhouette score histograms based on t-SNE visualization of the ECoG data. (Left) Wireless ECoG dataset. (Right) Wired ECoG dataset.

system for 7 days. In both recording setups, the rats were freely moving inside a $43 \times 33 \times 30$ cm $43 \times 33 \times 30$ cm cage. The sampling rates for the wired and wireless recordings were 30,000Hz and 512Hz, respectively.

4.1.2. Dataset Labeling and Construction

For the same subjects, electrical stimulation was applied to the motor cortex using a graphene-based electrode, as illustrated in Figure 1 (b). A total of 15 common channels were used for both wired and wireless measurements. Electrical stimulation was administered once per day to all rats. After one week of stimulation, the rats that received stimulation showed notable improvement in motor function, as confirmed by gait and other behavioral tests, compared to the unstimulated state. In addition, the ECoG recordings showed a decrease in high-frequency activity and an increase in low-frequency components after electrical stimulation. As a result, the dataset includes both normal-state ECoG signals (*i.e.*, post-stimulation) and Parkinsonian-state ECoG signals (*i.e.*, pre-stimulation). The detailed procedure for ECoG data acquisition is provided in the previous study (Shin et al., 2025).

A total of six rats were used in the experiments. For each subject, the state without electrical stimulation was defined as class 0, and the state after one week of continuous stimulation was defined as class 1, formulating the task as a binary classification problem. The class labels were determined based on behavioral tests conducted before and after electrical stimulation, following the procedure described in our previous study (Shin et al., 2025)

The wired ECoG data were downsampled from 30,000Hz to 512Hz, and both wired and wireless recordings were divided into 6-second non-overlapping

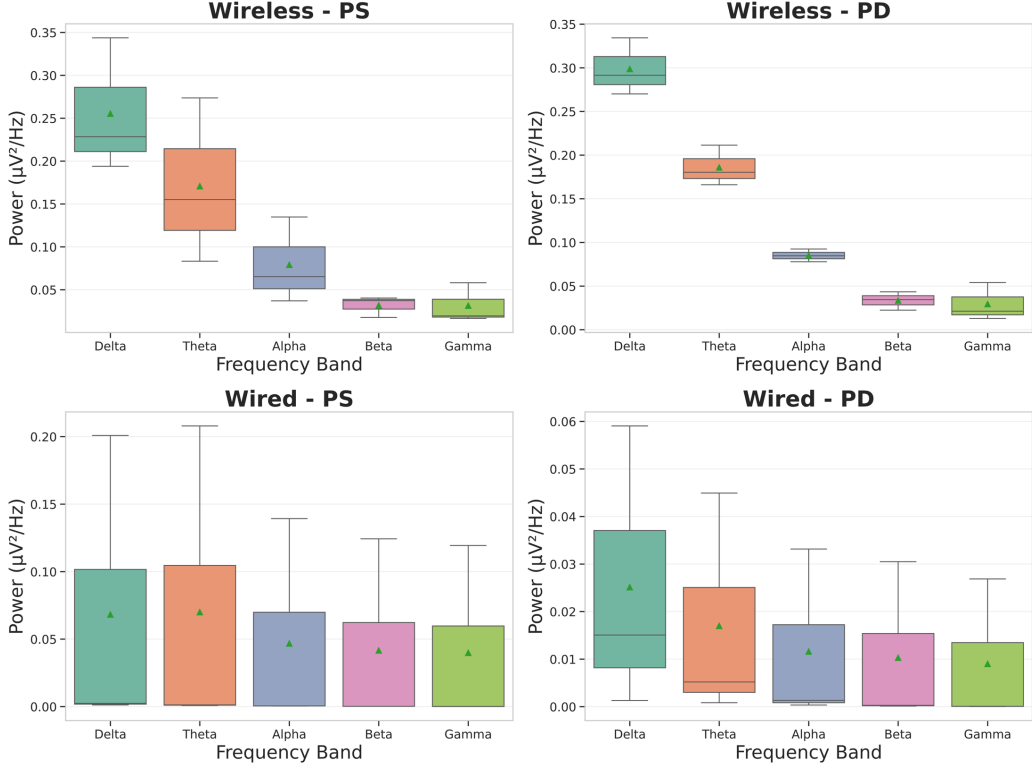


Figure 7: Power Spectral Density Analysis Across Different Datasets and Classes: Comparison of frequency band-specific PSD between wireless and wired in MOCOP dataset. PS denotes the Post-Stimulation state, while PD denotes Parkinson’s Disease.

segments. Table 1 presents the number of samples for each class and subject in the proposed ECoG dataset. In most subjects, the difference in the number of samples between the two classes was within 10%, except for Rat4, where the number of class 1 samples was approximately 30% higher than that of class 0. Finally, each dataset was divided into training, validation, and test sets with a ratio of 8:1:1.

4.1.3. Dataset Distribution Analysis

The proposed ECoG dataset was collected over an extended period while the rats were freely moving, which inevitably introduced movement artifacts and power-line noise. In addition, biological differences among individual rats lead to subject-specific variability. To analyze the biases across subjects and acquisition modalities, we computed the power spectral density (PSD)

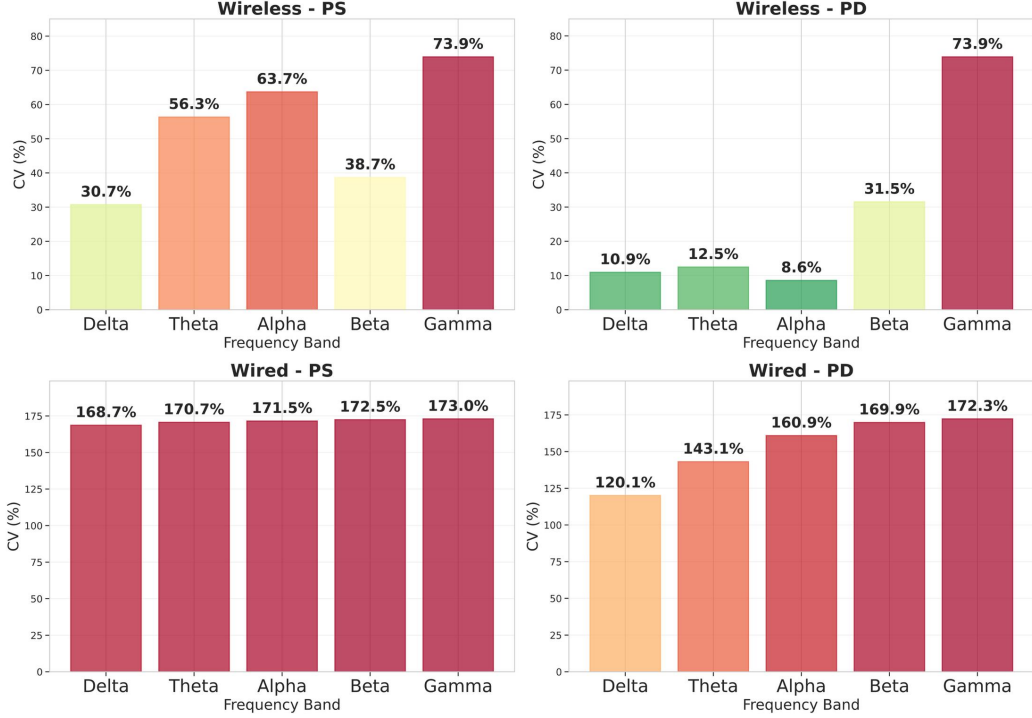


Figure 8: Inter-Subject Variability Analysis Using Coefficient of Variation (CV): Comparison of inter-subject variability between wireless and wired in MOCOP dataset. PS denotes the Post-Stimulation state, while PD denotes Parkinson's Disease.

(Kyllönen, 2024) of each recording and visualized the feature representations using t-SNE.

Figure 5 (a) and (b) show that the wired and wireless datasets form clearly separated clusters, indicating a substantial distributional difference between the two acquisition modalities. Figure 5 (c) and (d) show distinct inter-subject clustering within each modality. In addition, as shown in Figure 6, we quantitatively evaluated the degree of cluster separation using the silhouette score. The results show clear inter-subject clustering in both wired and wireless datasets, with greater subject-level variability observed in the wireless data.

Moreover, we quantitatively analyzed the PSD distributions across frequency bands and the inter-subject variability within the wired and wireless datasets. As shown in Figure 7, both datasets exhibited higher PSD values

in the low-frequency bands (*i.e.*, Delta, Theta, Alpha) than in the high-frequency bands (*i.e.*, Beta, Gamma). In both modalities, the PSD distributions differed before and after stimulation, indicating meaningful class-wise differences. Notably, the wireless data showed higher PSD values in the low-frequency bands, whereas the wired data exhibited relatively lower power. After stimulation, the wireless data showed an increase in Delta-band power, while the wired data showed a decrease in power across all frequency bands. These results highlight a clear distributional discrepancy between the wired and wireless datasets, suggesting the existence of a domain gap and emphasizing the need for domain generalization.

Figure 8 reports the coefficients of variation (CV) of the mean PSD across subjects. In the PD condition, both wired and wireless datasets exhibited high variability across subjects. After stimulation, variability in the wireless data decreased slightly in the low-frequency bands but remained substantial, whereas the wired data maintained consistently high variability across all bands. These results indicate substantial inter-subject variability and the need for generalization across subjects within each modality.

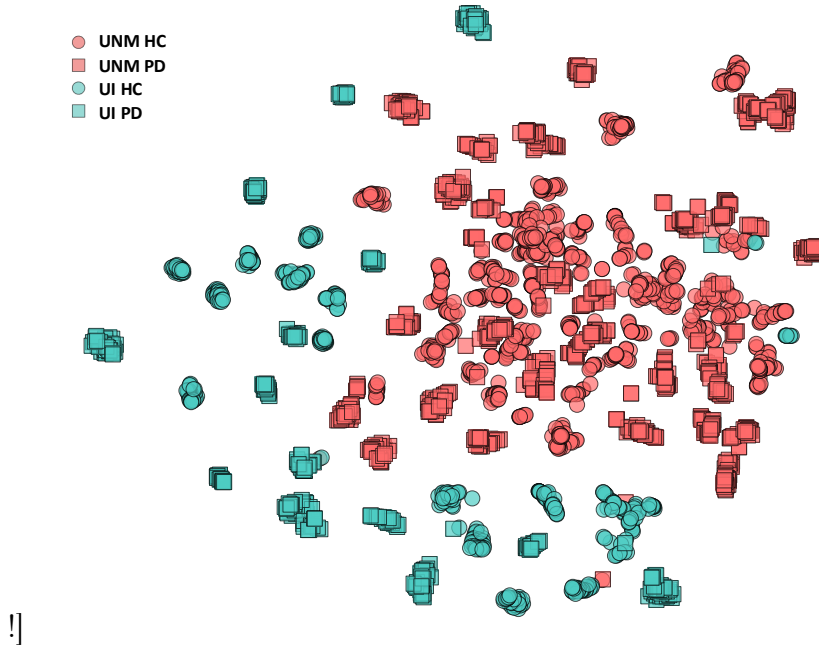


Figure 9: t-SNE visualization of the UI and UNM dataset after power spectral density (PSD) transformation.

	UI	UNM
Number of subject	28	52
Class 0 (Healthy control)	429	921
Class 1 (Parkinson's disease)	438	838

Table 2: Number of samples in the EEG datasets.

4.2. EEG Dataset

4.2.1. Data Acquisition from Previous Study

We utilized two publicly available EEG datasets that are widely used for PD classification (Cavanagh et al., 2018; Singh et al., 2020; Sugden and Diamandis, 2023): the University of New Mexico (UNM) and University of Iowa (UI) datasets. Both are commonly adopted as benchmark datasets for EEG-based Parkinson's disease diagnosis. A detailed description of each dataset is as follows:

1. **UNM Dataset:** This dataset consists of 52 participants, including 27 patients with PD and 25 healthy controls. EEG signals were collected both while the patients were on dopaminergic medication and after a 12-hour medication withdrawal period.
2. **UI Dataset:** This dataset consists of 28 participants, including 14 patients with PD and 14 healthy controls. EEG signals were collected only while the patients were on dopaminergic medication.

Both EEG datasets were recorded using a 64-channel BrainVision system at a sampling rate of 500 Hz. Detailed descriptions of the datasets are provided in the original publications (Cavanagh et al., 2018; Singh et al., 2020).

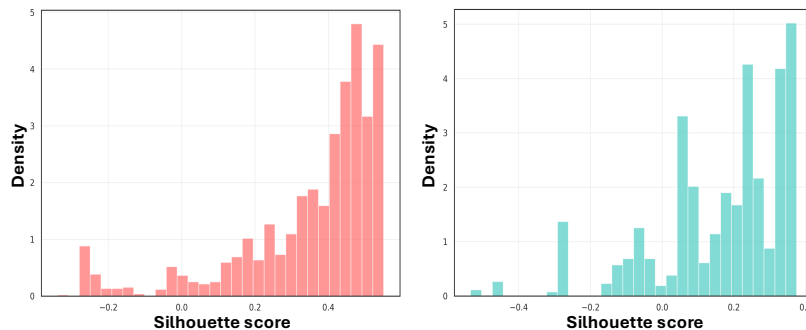


Figure 10: Silhouette score histograms based on t-SNE visualization of the EEG data. (Left) UNM dataset. (Right) UI dataset.

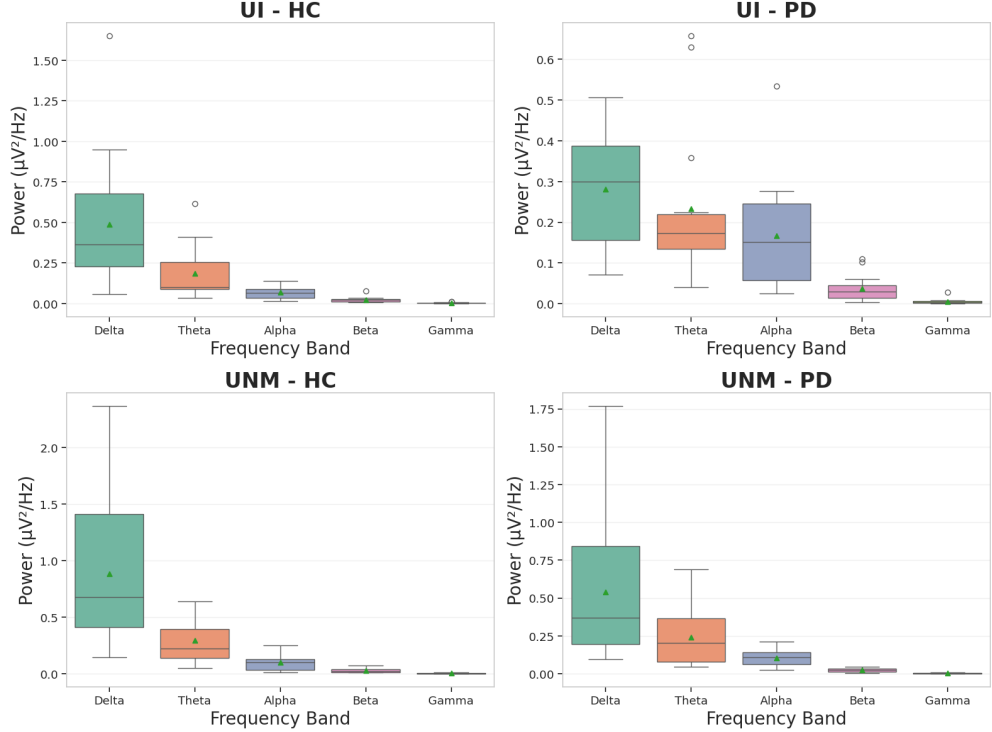


Figure 11: Power Spectral Density Analysis Across Different Datasets and Classes: Comparison of frequency band-specific PSD between UI and UNM in EEG dataset. HC denotes Healthy Control, while PD denotes Parkinson’s Disease.

In these datasets, preprocessing was performed following the procedures described in previous studies, and artifact subspace reconstruction (ASR) was not applied (Sugden and Diamandis, 2023). Electrodes that were not located at consistent positions across both datasets were excluded, resulting in 60 EEG channels used for analysis. After applying ISBCS, features from different subjects show lower inter-subject separability. Table 2 summarizes the number of subjects and samples in the UNM and UI datasets. Both datasets contain a relatively large number of subjects but a limited number of samples per subject. Although the two datasets have similar average participant ages, a considerable domain gap exists due to differences in recording locations, institutions, subject composition, medication status, and experimental protocols (Karakas and Latifoğlu, 2023). Figure 9 shows the t-SNE visualization of the PSD features, indicating a clear distributional discrepancy

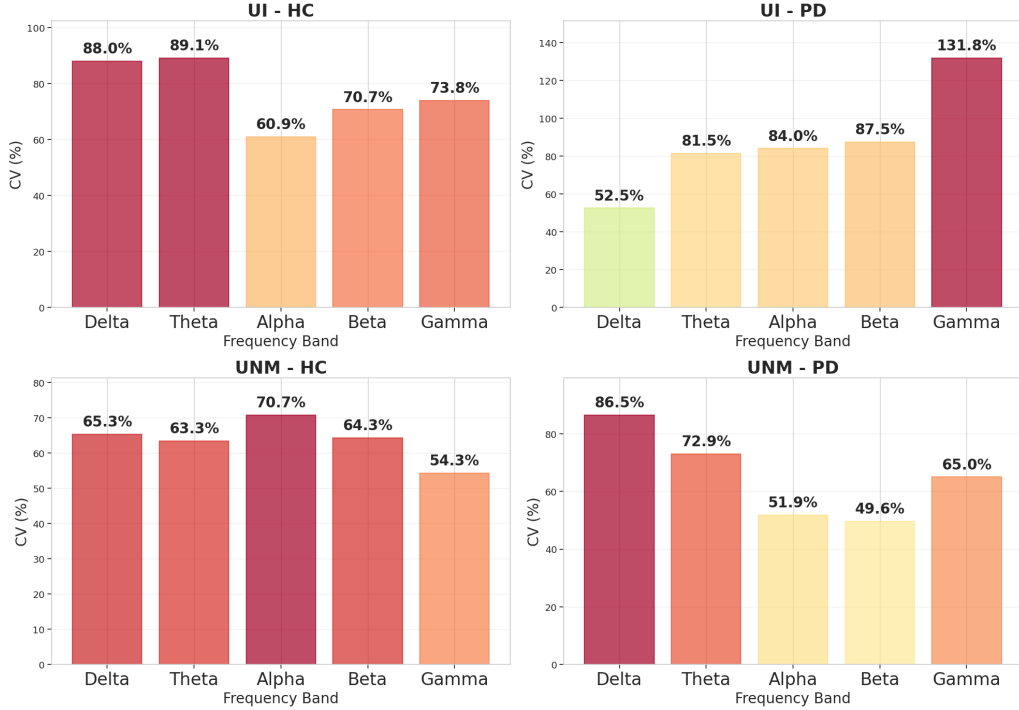


Figure 12: Inter-Subject Variability Analysis Using Coefficient of Variation (CV): Comparison of inter-subject variability between UI and UNM in EEG dataset. HC denotes Healthy Control, while PD denotes Parkinson’s Disease.

between the UNM and UI datasets. The silhouette score analysis (Figure 10) further supported this observation, revealing clear subject-wise clustering in both datasets. In addition, the UI dataset exhibited stronger inter-subject separation than the UNM dataset.

4.2.2. Dataset Distribution Analysis

Furthermore, we quantitatively analyzed the PSD distributions across frequency bands and the inter-subject variability within the UI and UNM datasets. During this analysis, extreme outliers were observed in the UNM data, particularly in the Delta and Theta bands. Therefore, we removed these outliers using the interquartile range (IQR) method, where values outside the range ($Q_1 - 1.5 \times IQR, Q_3 + 1.5 \times IQR$) for each frequency band were excluded.

As shown in Figure 11, both the UNM and UI datasets exhibited higher

PSD values in the low-frequency bands (*i.e.*, Delta, Theta, Alpha) than in the high-frequency bands (*i.e.*, Beta, Gamma). In both datasets, the PSD distributions differed between the PD and healthy control groups, showing distinct PSD patterns between the two populations. Notably, the UNM dataset showed overall higher PSD values in the low-frequency bands compared to the UI dataset. These distributional differences suggest a dataset-wise domain gap caused by variations in recording environments, institutions, and participant populations. These distributional differences indicate a domain discrepancy between the two datasets, likely arising from variations in recording environments and subject populations.

Figure 12 shows the CV of the mean PSD values for each subject. In the UI dataset, the healthy control and PD groups exhibited distinct variability patterns: the healthy control group showed higher variability in the low-frequency bands, whereas the PD group showed greater variability in the high-frequency range. In contrast, the UNM dataset displayed uniformly high CV values across all frequency bands for both groups. These findings reveal large inter-subject variability within both datasets

5. Experiments

5.1. Baselines

In this section, we compared the proposed method with the following two baseline models.

- **EEGNet** (Lawhern et al., 2018): A compact CNN architecture widely used for EEG signal classification. It extracts spatio-temporal features using depthwise and separable convolutions. In this study, EEGNet was used as a baseline model without any domain generalization approaches.
- **DDMR** (Wang et al., 2024b): A domain generalization model that leverages self-supervised learning to obtain subject-invariant representations. During pretraining, a multi-decoder autoencoder is used to extract invariant features, with Time Steps Shuffling-based noise injection to enhance robustness. In the fine-tuning phase, the pretrained encoder is integrated with a target classifier for downstream tasks.

Data type	Training dataset	Test dataset	Subject name	λ_{MI}	λ_{GRL}
ECoG dataset	Wireless	Wireless	Wireless Rat1	0.001	0.001
			Wireless Rat2	0.001	10.0
			Wireless Rat3	3.334	1.25
	Wired	Wired	Wired Rat1	4.445	2.084
			Wired Rat2	1.112	1.667
			Wired Rat3	0.001	0.417
	Wireless	Wired	Wired Rat1	1.667	0.001
			Wired Rat2	2.917	8.889
			Wired Rat3	3.334	4.445
EEG dataset	Wired	Wireless	Wireless Rat1	7.916	6.667
			Wireless Rat2	0.001	0.001
			Wireless Rat3	1.667	0.001
	UI	UNM	-	0.417	4.445
		UI	-	0.001	1.112

Table 3: Hyperparameter values of λ_{MI} and λ_{GRL} for each experimental setting.

5.2. Evaluation Metrics

In this study, we evaluated binary classification performance using multiple metrics (*i.e.*, accuracy, recall, precision, and F1 score). All metrics were computed using macro-averaging, where scores were calculated for each class and then averaged. These metrics followed standard definitions commonly used for classification tasks.

5.3. Implementation details

ASR Preprocessing Settings. To suppress artifacts in both ECoG and EEG data, we used the Artifact Subspace Reconstruction (ASR) function implemented in EEGLAB’s clean_asr() module. All ASR parameters were kept at their default settings for both datasets without additional tuning.

Parameter Settings For EEGNet, the temporal kernel length was set to half of the sampling rate, as suggested in the original paper. (*i.e.*, ECoG: 256 HZ, EEG: 250 HZ) The number of channels was set to match those available in each dataset. For the proposed method, we conducted a grid search over two hyperparameters, λ_{MI} and λ_{GRL} , uniformly sampled within the range [0.001, 10] using 25 and 10 intervals, respectively. The optimal values for each training dataset were selected based on this search, and the final configurations are summarized in Table 3.

Optimization Settings. All models were trained using the Adam optimizer with an initial learning rate of 0.001, while other hyperparameters

	Data type	Training dataset	Test dataset	Goal
Experiment 1	ECoG	Wireless	Wireless	Model performance on unseen subjects
		Wired	Wired	(Inter-subject generalization)
Experiment 2	ECoG	Wireless	Wired	Model performance on unseen domains
		Wired	Wireless	(Inter-modality generalization)
Experiment 3	ECoG	Wireless	Wireless	
		Wired	Wired	
		Wireless	Wired	Ablation study
		Wired	Wireless	
Experiment 4	EEG	UI	UNM	Model performance on unseen domains
		UNM	UI	(Inter-domain generalization)

Table 4: Summary of experiments. This table presents experimental setup for evaluating model performance. Experiments 1 and 2 investigate inter-subject and inter-modality generalization using ECoG data. Experiment 3 shows the results of an ablation study. Experiment 4 examines inter-domain generalization using EEG data.

were kept at their default values. The learning rate was dynamically adjusted by a scheduler, which reduced it by half if the target macro-accuracy did not improve by more than 0.001 for five successive epochs on the validation set. To ensure convergence, each model was trained for at least 20 epochs, and early stopping with a patience of 10 was applied to prevent overfitting.

5.4. Summary of Experiments

Four experiments were conducted on the ECoG dataset as described below. Experiments 1 and 2 evaluated the effects of inter-subject and inter-modality generalization within the ECoG dataset, respectively. Experiment 3 conducted an ablation study to evaluate the effectiveness and compatibility of the proposed ISBCS and Domain Adversarial Learning (DAL) modules. Finally, Experiment 4 further validated the generalization capability of the proposed method using a publicly available EEG dataset, as summarized in Table 4

5.5. Results on Domain generalization (ECoG dataset)

Experiments 1

Figure 13 compares the inter-subject generalization performance of the proposed method with the baseline models on the ECoG dataset under both wireless and wired conditions. The results show that the proposed framework outperforms the baseline models in terms of all four evaluation metrics for

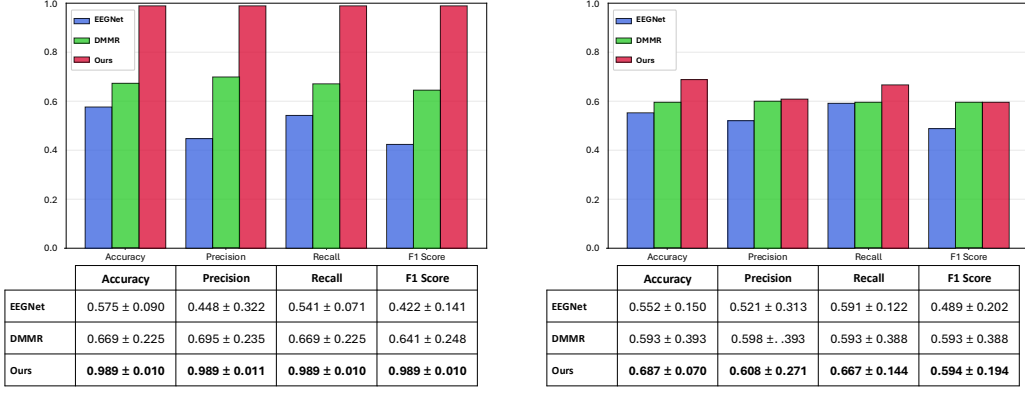


Figure 13: Results of Experiments 1: (Left) Wireless (train) → cross-subject test (wireless); (Right) Wired (train) → cross-subject test (wired).

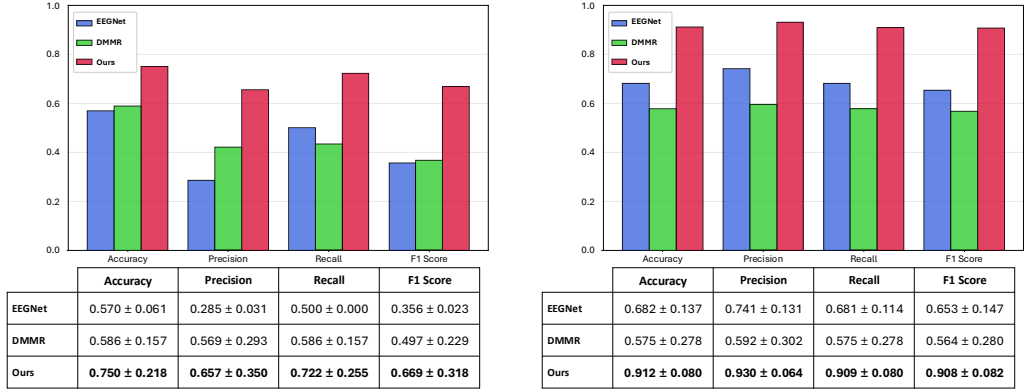


Figure 14: Results of Experiments 2: (Left) Wireless (train) → transfer to wired (cross-subject); (Right) Wired (train) → transfer to wireless (cross-subject).

unseen subjects, indicating its superior generalization capability. Specifically, in the wireless setting, the proposed method achieved a substantial improvement of approximately 41% in macro-accuracy over EEGNet. Notably, the performance gain was greater in the wireless setting, where inter-subject distributional discrepancy was more significant, indicating that the proposed method achieves stronger domain generalization under higher inter-subject variability.

Experiments 2

In addition, we validated the effectiveness of the proposed method in an inter-modality generalization setting, a more challenging task that involves not only inter-subject variability but also domain discrepancies caused by differences in recording modalities (*e.g.*, sampling rate, noise). Figure 14 presents the results of inter-modality transfer between wireless and wired recordings, including transfers from wireless to wired and from wired to wireless. The proposed method consistently outperformed the baseline across all metrics in both transfer settings. In particular, when transferring from wired to wireless recordings, it achieved a macro-accuracy of 91.2%, compared to 68.2% achieved by EEGNet. These results indicate that the proposed method remains effective under compounded inter-modality shifts.

5.6. Results on Ablation Study

Experiments 3

Figure 15 presents the ablation results to validate the contributions of ISBCS and DAL. Applying either component alone improved performance across all settings. When trained on wired data (Figure 15 (a), (c)), the ISBCS-only model achieved higher accuracy than the DAL-only model, whereas the opposite trend was observed when trained on wireless data. These results suggest that the two components respond differently to variations in recording modalities and domain characteristics. Combining ISBCS and DAL achieved the highest performance across all settings, demonstrating that the two components work in a complementary manner.

To better understand the impact of ISBCS on the feature space, we analyzed its effect using t-SNE visualization.

Figure 16 visualizes the feature distributions extracted by the proposed framework from two types of inputs: the original data and the ISBCS-augmented data using t-SNE visualization. For the original data, features from different subjects are relatively well separated in the t-SNE space. After applying ISBCS, however, the features become less distinguishable across subjects, indicating that ISBCS effectively mitigates subject-specific characteristics through inter-subject channel exchange. To quantitatively assess the degree of inter-subject separability, we computed the F-statistic, which measures the ratio of between-subject variance to within-subject variance. For the original data, the F-statistic was 24.48, indicating significant subject-specific differences. After applying ISBCS augmentation, the F-statistic dramatically decreased to 0.99, which indicates negligible between-subject differences. This

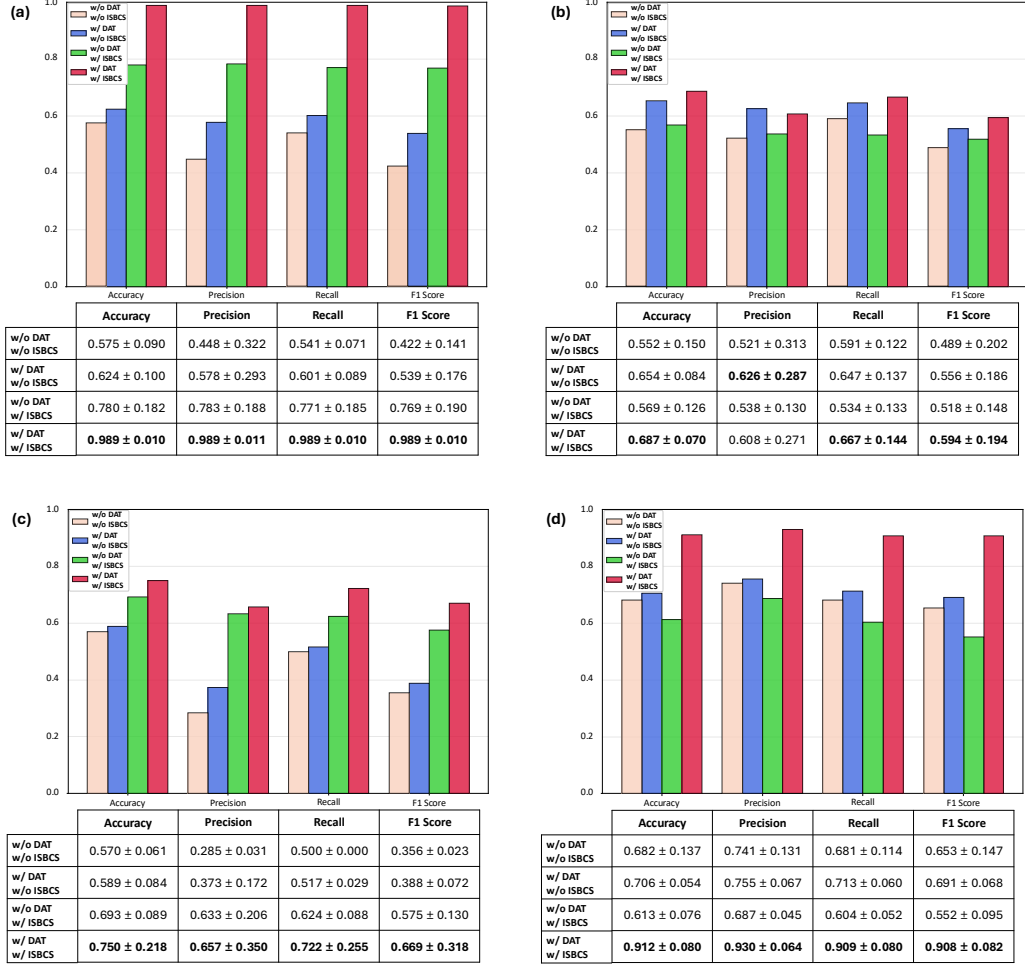


Figure 15: Results of Experiments 3: (a) Wireless (train) → Wireless (cross-subject test), (b) Wired (train) → Wired (cross-subject test), (c) Wireless (train) → Wired (cross-subject transfer), (d) Wired (train) → Wireless (cross-subject transfer).

reduction provides statistical evidence that ISBCS effectively reduces inter-subject variability.

5.7. Results on Domain generalization (Public EEG dataset)

Experiments 4

We further evaluated the proposed method on publicly available EEG datasets to examine its cross-modality generalization. This setting is par-

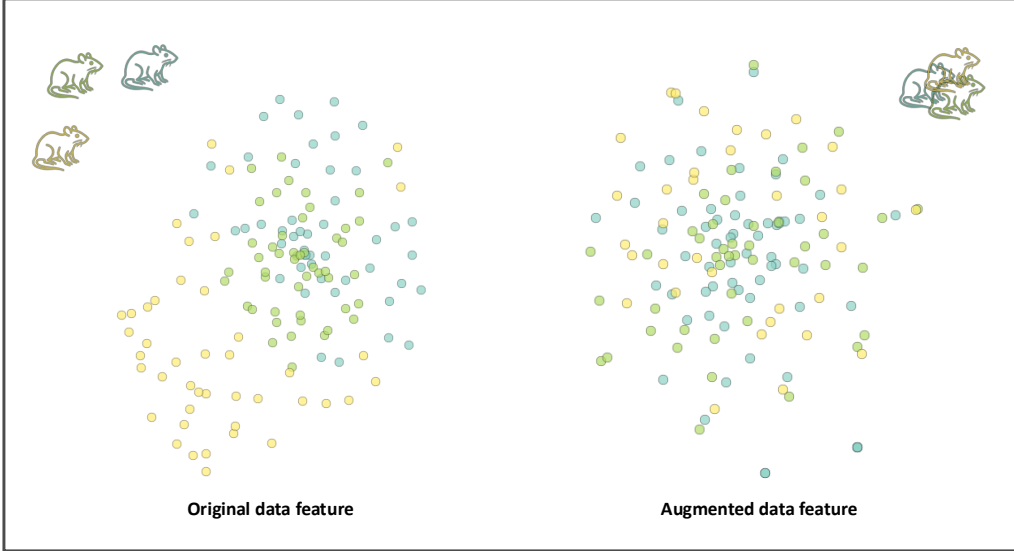


Figure 16: t-SNE visualization of the original and ISBCS-augmented data features. Each dot represents a sample in the feature space, and different colors correspond to different subjects.

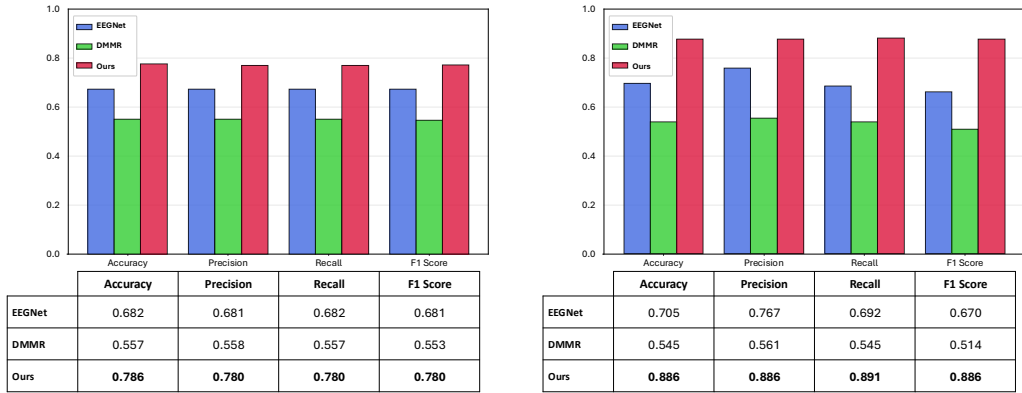


Figure 17: Results of Experiments 4: (Left) UI (train) → UNM (cross-subject test); (Right) UNM (train) → UI (cross-subject test).

ticularly challenging due to compounded domain differences across subjects, recording modalities, institutions, medication states, and environments. Figure 17 presents the cross-dataset evaluation results between the UI and UNM datasets. Compared to EEGNet, DMMR showed lower macro-accuracy, indi-

cating limited domain generalization capability under compounded domain variations. In contrast, the proposed method consistently outperformed the baselines across all experimental settings. Notably, when trained on the UNM dataset and tested on the UI dataset, it achieved approximately a 32% improvement in macro-accuracy over EEGNet. These results indicate that the proposed method exhibits strong generalization and transferability across diverse and complex domain variations.

6. Discussion

6.1. Key findings

Previous ECoG-based classification models have mainly focused on performance optimization rather than robustness to domain shifts. To address this limitation, we present the first domain generalization framework for ECoG-based Parkinson’s disease classification, which enables learning of domain-invariant representations. The proposed method shows strong domain generalization capability not only on ECoG data but also on EEG signals, indicating its effectiveness across different types of brain signals.

This study aims to reduce various domain discrepancies inherent in brain-signal data, including inter-subject physiological variability, sensor characteristics, and differences in recording environments. To this end, we combine the pre-processing augmentation method Inter-Subject Balanced Channel Swap (ISBCS) with the in-processing domain adversarial learning approach.

To evaluate the effectiveness of the two methods, we conducted extensive experiments on the individual contributions of ISBCS and domain adversarial learning. In the wireless dataset, which exhibits large inter-subject variability, ISBCS contributed more significantly than domain adversarial learning. Conversely, in the wired dataset with relatively small variability, the effect of ISBCS was more limited. These results suggest that an appropriate generalization strategy depends on the characteristics of the data and that the two components of the proposed framework work in a complementary manner, minimizing classification degradation while enhancing generalization capability.

To evaluate the effectiveness of ISBCS and domain adversarial learning, we conducted extensive experiments to examine their individual contributions. In the wireless dataset, which shows large inter-subject variability, ISBCS contributed more significantly than domain adversarial learning. Conversely, in the wired dataset with relatively small variability, ISBCS had a

smaller impact. These results suggest that an effective domain generalization strategy may vary across different conditions. Our framework leverages both ISBCS and domain adversarial learning, which work in a complementary manner, preserving classification ability while enhancing overall generalization capability.

6.2. Limitations and Future Work

This study focused on domain generalization for Parkinson’s disease prediction based on ECoG and EEG data. Future research can be extended in several directions as follows.

This study focused on domain generalization based on brain signals for Parkinson’s disease prediction. Future work will extend the proposed framework to broader BCI applications, including emotion recognition and neurological disorder analysis, thereby broadening its applicability to general cognitive and clinical research using brain signals.

In addition, the proposed method was designed based on EEGNet, a lightweight neural network model that is widely used in the BCI domain. It is expected to be applicable to other neural architectures, such as EEG Conformer (Song et al., 2023) and EEG-TCNet (Ingolfsson et al., 2020). However, considering the recent trend toward deeper and Transformer-based architectures, extending the proposed framework to more complex and large-scale models will be an important direction for future research.

Lastly, the proposed method involves two key hyperparameters, λ_{GRL} and λ_{MI} , which significantly affect performance within domain adversarial learning. Such hyperparameter sensitivity has also been observed in previous adversarial learning and domain generalization studies(Ganin et al., 2016; Yang et al., 2020). Future work will investigate strategies for setting appropriate initial values of λ_{GRL} and λ_{MI} or treating them as learnable parameters that can be dynamically optimized during training.

7. Conclusion

This study addressed the domain generalization problem in Parkinson’s disease prediction using ECoG signals by constructing the first publicly available ECoG benchmark dataset and proposing a method for learning domain-invariant representations. The proposed method combines Inter-Subject Balanced Channel Swap (ISBCS) and domain adversarial learning in a complementary manner, achieving superior performance across various domain-shift

scenarios, such as cross-subject and cross-modality evaluations. In particular, it improved macro-accuracy by up to 41% over the baseline in cross-subject evaluations. These results demonstrate that the proposed method effectively learns domain-invariant features under diverse domain variations. Furthermore, cross-dataset evaluations on public EEG benchmarks (*i.e.*, UI and UNM) showed that the method generalizes beyond ECoG to EEG signals, suggesting its potential as a unified framework for electrophysiological signal analysis. To facilitate further research in this direction, we have publicly released the constructed ECoG benchmark and source code. We expect that future work will advance this method by extending it to other neurological disorders, incorporating state-of-the-art architectures, and developing effective strategies for optimizing key hyperparameters.

CRediT authorship contribution statement

Seongwon Jin: Writing - original draft, Software, Visualization, Validation, Data curation, Conceptualization. **Hanseul Choi:** Writing - original draft, Visualization, Data curation, Conceptualization. **Sunggu Yang:** Resources. **Sungho Park:** Writing review & editing, Supervision, Conceptualization. **Jibum Kim:** Funding acquisition, Writing review & editing, Project administration, Supervision, Conceptualization.

Acknowledgements

This work was supported by the National Research Foundation of Korea (NRF) Grant funded by Korea Government through the Ministry of Science and ICT (MSIT) under Grant RS-2024-00341307. This work was also supported by Incheon National University Research Grant in 2024.

References

Abumaloh, R.A., Nilashi, M., Samad, S., Ahmadi, H., Alghamdi, A., et al., 2024. Parkinson's disease diagnosis using deep learning: A bibliometric analysis and literature review. Ageing Res Rev. 96, 102285. <https://doi.org/10.1016/j.arr.2024.102285>.

Agrawal, S., Sahu, S.P., 2025. Quantitative EEG-Based Regional Spectral Analysis for Parkinson's Disease Detection, In: 2025 IEEE

International Conference on Interdisciplinary Approaches in Technology and Management for Social Innovation, Vol. 3. pp. 1-6. <https://doi.org/10.1109/IATMSI64286.2025.10985366>.

Ali, A.A.N., Alam, M., Klein, S.C., Behmann, N., Krauss, J.K., et al., 2022. Predictive accuracy of CNN for cortical oscillatory activity in an acute rat model of parkinsonism. *Neural Networks*. 146, 334–340. <https://doi.org/10.1016/j.neunet.2021.11.025>.

Arjovsky, M., Bottou, L., Gulrajani, I., Lopez-Paz, D., 2020. Invariant risk minimization. arXiv preprint. <https://doi.org/10.48550/arXiv.1907.02893>.

Benabid, A.L., Chabardes, S., Mitrofanis, J., Pollak, P., 2009. Deep brain stimulation of the subthalamic nucleus for the treatment of Parkinson's disease. *Lancet Neurol*. 8 (1), 67-81. [https://doi.org/10.1016/S1474-4422\(08\)70291-6](https://doi.org/10.1016/S1474-4422(08)70291-6).

Blum, S., Jacobsen, N.S.J., Bleichner, M.G., Debener, S., 2019. A riemannian modification of artifact subspace reconstruction for EEG artifact handling. *Front Hum Neurosci*. 13, 141. <https://doi.org/10.3389/fnhum.2019.00141>.

Bore, J.C., Campbell, B.A., Cho, H., Gopalakrishnan, R., Machado, A.G., et al., 2020. Prediction of mild Parkinsonism revealed by neural oscillatory changes and machine learning. *J Neurophysiol*. 124 (6), 1698-1705. <https://doi.org/10.1152/jn.00534.2020>.

Calvo Peiro, N., Haugland, M.R., Kutuzova, A., Graef, C., Bocum, A., et al., 2025. Deep Learning-Driven EEG Analysis for Personalized Deep Brain Stimulation Programming in Parkinson's Disease. medRxiv preprint. <https://doi.org/10.1101/2025.02.11.25321886>.

Cataldo, A., Criscuolo, S., De Benedetto, E., Masciullo, A., Pesola, M., Schiavoni, R., Invitto, S., 2022. A method for optimizing the artifact subspace reconstruction performance in low-density EEG. *IEEE Sens J*. 22 (21), 21257–21265. <https://doi.org/10.1109/JSEN.2022.3208768>.

Cavanagh, J.F., Kumar, P., Mueller, A.A., Richardson, S.P., Mueen, A., 2018. Diminished EEG habituation to novel events effectively classifies Parkinson's patients. *Clin Neurophysiol*. 129 (2), 409–418. <https://doi.org/10.1016/j.clinph.2017.11.023>.

Chang, C.Y., Hsu, S.H., Pion-Tonachini, L., Jung, T.P., 2018. Evaluation of artifact subspace reconstruction for automatic EEG artifact removal. In: 2018 40th annual international conference of the IEEE engineering in medicine and biology society (EMBC). pp. 1242-1245.

Chen, J., Chen, X., Wang, R., Le, C., Khalilian-Gourtani, A., Jensen, E., Dugan, P., Doyle, W., Devinsky, O., Friedman, D., Flinker, A., Wang, Y., 2025. Transformer-based neural speech decoding from surface and depth electrode signals. *J Neural Eng* 22. <https://doi.org/10.1088/1741-2552/adab21>

Cheng, X., Xie, Y., 2024. Kernel two-sample tests for manifold data. 30 (4), 2572-2597. <https://doi.org/10.3150/23-BEJ1685>.

Cui, X., Cao, J., Lai, X., Jiang, T., Gao, F., 2022. Cluster embedding joint-probability-discrepancy transfer for cross-subject seizure detection. *IEEE Trans Neural Syst Rehabil Eng.* 31, 593–605. <https://doi.org/10.1109/TNSRE.2022.3229066>.

Cui, J., Yuan, L., Wang, Z., Li, R., Jiang, T., 2023. Towards best practice of interpreting deep learning models for EEG-based brain computer interfaces. *Front Comput Neurosci.* 17, 1232925. <https://doi.org/10.3389/fncom.2023.1232925>.

Dayal, A., KB, V., Cenkeramaddi, L.R., Mohan, C., Kumar, A., et al., 2023. MADG: margin-based adversarial learning for domain generalization. *Adv Neural Inf Process Syst.* 36, 58938-58952.

Dayanik, E., Padó, S., 2021. Disentangling document topic and author gender in multiple languages: Lessons for adversarial debiasing. In: Proceedings of the Eleventh Workshop on Computational Approaches to Subjectivity, Sentiment and Social Media Analysis. pp. 50-61.

Dorsey, E.R., Elbaz, A., Nichols, E., Abd-Allah, F., Abdelalim, A., et al., 2018. Global, regional, and national burden of Parkinson's disease, 1990–2016: a systematic analysis for the Global Burden of Disease Study 2016. *Lancet Neurol.* 17 (11), 939–953. [https://doi.org/10.1016/S1474-4422\(18\)30295-3](https://doi.org/10.1016/S1474-4422(18)30295-3).

Dragomiretskiy, K., Zosso, D., 2014. Variational mode decomposition. *IEEE Trans Signal Process.* 62 (3), 531–544. <https://doi.org/10.1109/TSP.2013.2288675>.

Ganin, Y., Ustinova, E., Ajakan, H., Germain, P., Larochelle, H., et al., 2016. Domain-adversarial training of neural networks. *J Mach Learn Res.* 17 (59), 1-35.

Haufe, S., Deguzman, P., Henin, S., Arcaro, M., Honey, C.J., et al., 2018. Elucidating relations between fMRI, ECoG, and EEG through a common natural stimulus. *NeuroImage.* 179, 79-81. <https://doi.org/10.1016/j.neuroimage.2018.06.016>.

Huang, N.E., Shen, Z., Long, S.R., Wu, M.C., Shih, H.H., et al., 1998. The empirical mode decomposition and the Hilbert spectrum for nonlinear and non-stationary time series analysis, In: *Proceedings of the Royal Society of London. Series A: mathematical, physical and engineering sciences*, vol. 454, no 1971. pp. 903-995. <https://doi.org/10.1098/rspa.1998.0193>.

Huang, G., Zhao, Z., Zhang, S., Hu, Z., Fan, J., et al., 2023. Discrepancy between inter- and intra-subject variability in EEG-based motor imagery brain-computer interface: Evidence from multiple perspectives. *Front Neurosci.* 17, 1122661. <https://doi.org/10.3389/fnins.2023.1122661>.

Ingolfsson, T. M., Hersche, M., Wang, X., Kobayashi, N., Cavigelli, L., et al., 2020. EEG-TCNet: An accurate temporal convolutional network for embedded motor-imagery brain-machine interfaces. In: *2020 IEEE International Conference on Systems, Man, and Cybernetics (SMC)*. pp. 2958-2965.

Jeong, D.H., Kim, Y. Do, Song, I.U., Chung, Y.A., Jeong, J., 2016. Wavelet energy and wavelet coherence as eeg biomarkers for the diagnosis of Parkinson's disease-related dementia and Alzheimer's disease. *Entropy.* 18 (1). <https://doi.org/10.3390/e18010008>.

Ji, C., 2024. Bi-Band ECoGNet for ECoG Decoding on Classification Task. arXiv preprint. <https://doi.org/10.48550/arXiv.2412.00378>.

Kalia, L.V., Lang, A.E., 2015. Parkinson's disease. *Lancet.* 386 (9996), 896-912. [https://doi.org/10.1016/S0140-6736\(14\)61393-3](https://doi.org/10.1016/S0140-6736(14)61393-3).

Kamnitsas, K., Baumgartner, C., Ledig, C., Newcombe, V.F.J., Simpson, J.P., et al., 2016. Unsupervised domain adaptation in brain lesion segmentation with adversarial networks. In: International conference on information processing in medical imaging. Springer, pp. 597-609. https://doi.org/10.1007/978-3-319-59050-9_47.

Kamycki, K., Kapuscinski, T., Oszust, M., 2020. Data augmentation with suboptimal warping for time-series classification. *Sensors.* 20 (1), 98. <https://doi.org/10.3390/s20010098>.

Kanth, S.T., Ray, S., 2020. Electrocorticogram (ECOG) is highly informative in primate visual cortex. *J Neurosci.* 40 (12), 2430–2444. <https://doi.org/10.1523/JNEUROSCI.1368-19.2020>.

Karakaş, M.F., Latifoğlu, F., 2023. Distinguishing Parkinson's disease with GLCM features from the hankelization of EEG signals. *Diagnostics.* 13 (10), 1769. <https://doi.org/10.3390/diagnostics13101769>.

Karpiel, I., Kurasz, Z., Kurasz, R., Duch, K., 2021. The influence of filters on EEG-ERP testing: Analysis of motor cortex in healthy subjects. *Sensors.* 21 (22), 7711. <https://doi.org/10.3390/s21227711>.

Kim, B., Kim, H., Kim, K., Kim, S., Kim, J., 2019. Learning not to learn: Training deep neural networks with biased data. In: Proceedings of the IEEE/CVF conference on computer vision and pattern recognition. pp. 9012-9020.

Kim, J., Choi, H., Kim, G., Yang, S., Baeg, E., et al., 2025. Explainable AI-Driven Neural Activity Analysis in Parkinsonian Rats under Electrical Stimulation. arXiv preprint. <https://doi.org/10.48550/arXiv.2502.12471>.

Kumaravel, V.P., Kartsch, V., Benatti, S., Vallortigara, G., Farella, E., et al., 2021. Efficient artifact removal from low-density wearable EEG using artifacts subspace reconstruction. In: 2021 43rd annual international conference of the IEEE engineering in medicine & biology society (EMBC). pp. 333–336. <https://doi.org/10.1109/EMBC46164.2021.9629771>.

Kyllönen, M., 2024. Unsupervised representation learning visualization for brain activity dynamics in REM-sleep.

Lachaux, J.P., Axmacher, N., Mormann, F., Halgren, E., Crone, N.E., 2012. High-frequency neural activity and human cognition: Past, present and possible future of intracranial EEG research. *Prog Neurobiol.* 98 (3), 279-301. <https://doi.org/10.1016/j.pneurobio.2012.06.008>.

Lam, V., Oliugbo, C., Parida, A., Linguraru, M.G., Anwar, S.M., 2024. Self-supervised learning for seizure classification using ECoG spectrograms. In: *Medical Imaging 2024: Computer-Aided Diagnosis*, Vol. 12927. pp. 597-602. <https://doi.org/10.1117/12.3007431>.

Lawhern, V.J., Solon, A.J., Waytowich, N.R., Gordon, S.M., Hung, C.P., et al., 2018. EEGNet: A compact convolutional neural network for EEG-based brain-computer interfaces. *J Neural Eng.* 15 (5), 056013. <https://doi.org/10.1088/1741-2552/aace8c>.

Li, H., Pan, S.J., Wang, S., Kot, A.C., 2018. Domain generalization with adversarial feature learning. In: *Proceedings of the IEEE conference on computer vision and pattern recognition*. pp. 5400-5409.

Little, S., Pogosyan, A., Neal, S., Zavala, B., Zrinzo, L., et al., 2013. Adaptive deep brain stimulation in advanced Parkinson disease. *Ann Neurol.* 74 (3), 449–457. <https://doi.org/10.1002/ana.23951>.

Ma, B.Q., Li, H., Zheng, W.L., Lu, B.L., 2019. Reducing the subject variability of eeg signals with adversarial domain generalization, In: *International Conference on Neural Information Processing*. Springer, pp. 30–42. https://doi.org/10.1007/978-3-030-36708-4_3.

Makeig, S., Jung, T.P., Bell, A.J., Sejnowski, T.J., 1995. Independent component analysis of electroencephalographic data. *Adv Neural Inf Process Syst.* 8.

Melbaum, S., Russo, E., Eriksson, D., Schneider, A., Durstewitz, D., et al., 2022. Conserved structures of neural activity in sensorimotor cortex of freely moving rats allow cross-subject decoding. *Nat Commun.* 13 (1), 7420. <https://doi.org/10.1038/s41467-022-35115-6>.

Memar, M.O., Ziae, N., Nazari, B., Yousefi, A., 2025. RISE-iEEG: Robust to Inter-Subject Electrodes Implantation Variability iEEG Classifier. *arXiv preprint*. <https://doi.org/10.48550/arXiv.2408.14477>.

Miller, K.J., Schalk, G., Fetz, E.E., Den Nijs, M., Ojemann, J.G., Rao, R.P.N., 2010. Cortical activity during motor execution, motor imagery, and imagery-based online feedback. *Proc Natl Acad Sci.* 107 (9), 4430–4435. <https://doi.org/10.1073/pnas.0913697107>.

Muandet, K., Balduzzi, D., Schölkopf, B., 2013. Domain generalization via invariant feature representation. In: International conference on machine learning, PMLR. pp. 10-18.

Mullen, T.R., Kothe, C.A.E., Chi, Y.M., Ojeda, A., Kerth, T., et al., 2015. Real-time neuroimaging and cognitive monitoring using wearable dry EEG. *IEEE Trans Biomed Eng.* 62 (11), 2553–2567. <https://doi.org/10.1109/TBME.2015.2481482>.

Neves, C., Zeng, Y., Xiao, Y., 2024. Parkinson's disease detection from resting state EEG using multi-head graph structure learning with gradient weighted graph attention explanations. In: International Workshop on Machine Learning in Clinical Neuroimaging. Springer, pp. 3-12. https://doi.org/10.1007/978-3-031-78761-4_1.

Nolan, H., Whelan, R., Reilly, R.B., 2010. FASTER: fully automated statistical thresholding for EEG artifact rejection. *J Neurosci Methods.* 192 (1), 152–162. <https://doi.org/10.1016/j.jneumeth.2010.07.015>.

Obayya, M., Saeed, M.K., Maashi, M., Alotaibi, S.S., Salama, A.S., et al., 2023. A novel automated Parkinson's disease identification approach using deep learning and EEG. *PeerJ Comput Sci.* 9, e1663. <https://doi.org/10.7717/peerj-cs.1663>.

Obeso, J.A., Stamelou, M., Goetz, C.G., Poewe, W., Lang, A.E., et al., 2017. Past, present, and future of Parkinson's disease: A special essay on the 200th Anniversary of the Shaking Palsy. *Mov Disord.* 32 (9), 1264-1310. <https://doi.org/10.1002/mds.27115>.

Oh, S.L., Hagiwara, Y., Raghavendra, U., Yuvaraj, R., Arunkumar, N., et al., 2020. A deep learning approach for Parkinson's disease diagnosis from EEG signals. *Neural Comput Appl.* 32 (15), 10927–10933. <https://doi.org/10.1007/s00521-018-3689-5>.

Palmer, J.A., Kreutz-Delgado, K., Makeig, S., 2012. AMICA: An adaptive mixture of independent component analyzers with shared components.

Swartz Center for Computational Neuroscience. University of California San Diego, Tech Rep.

Reddi, S.J., Ramdas, A., Póczos, B., Singh, A., Wasserman, L., 2015. On the high dimensional power of a linear-time two sample test under mean-shift alternatives. In: Artificial Intelligence and Statistics, PMLR. pp. 772–780.

Rommel, C., Moreau, T., Paillard, J., Gramfort, A., 2022. CADDA: Class-wise automatic differentiable data augmentation for EEG signals. arXiv preprint. <https://doi.org/10.48550/arXiv.2106.13695>.

Sagawa, S., Koh, P.W., Hashimoto, T.B., Liang, P., 2019. Distributionally robust neural networks for group shifts: On the importance of regularization for worst-case generalization. arXiv preprint. <https://doi.org/10.48550/arXiv.1911.08731>.

Schlögl, A., Pfurtscheller, G., Schack, B., 1996. Single-trial EEG analysis using an adaptive autoregressive model. In: Proceedings of Fourth International Symposium on Central Nervous Monitoring.

Shah, S.A.A., Zhang, L., Bais, A., 2020. Dynamical system based compact deep hybrid network for classification of Parkinson disease related EEG signals. *Neural Networks*. 130, 75–84. <https://doi.org/10.1016/j.neunet.2020.06.018>.

Shankar, S., Piratla, V., Chakrabarti, S., Chaudhuri, S., Jyothi, P., et al, 2018. Generalizing across domains via cross-gradient training. arXiv preprint. <https://doi.org/10.48550/arXiv.1804.10745>.

Shin, H., Kim, K., Lee, J., Nam, J., Baeg, E., et al., 2025. A Wireless Cortical Surface Implant for Diagnosing and Alleviating Parkinson’s Disease Symptoms in Freely Moving Animals. *Adv Healthc Mater.* 14 (17). <https://doi.org/10.1002/adhm.202405179>.

Singh, A., Cole, R.C., Espinoza, A.I., Brown, D., Cavanagh, J.F., et al., 2020. Frontal theta and beta oscillations during lower-limb movement in Parkinson’s disease. *Clin Neurophysiol.* 131 (3), 694–702. <https://doi.org/10.1016/j.clinph.2019.12.399>.

Somervail, R., Cataldi, J., Stephan, A.M., Siclari, F., Iannetti, G.D., 2023. Dusk2Dawn: an EEGLAB plugin for automatic cleaning of whole-night

sleep electroencephalogram using Artifact Subspace Reconstruction. *Sleep*. 46 (12), zsad208. <https://doi.org/10.1093/sleep/zsad208>.

Song, Y., Zheng, Q., Liu, B., Gao, X., 2023. EEG conformer: Convolutional transformer for EEG decoding and visualization. *IEEE Trans Neural Syst Rehabil Eng* 31, 710–719. <https://doi.org/10.1109/TNSRE.2022.3230250>.

Srinivasan, R., Winter, W.R., Ding, J., Nunez, P.L., 2007. EEG and MEG coherence: Measures of functional connectivity at distinct spatial scales of neocortical dynamics. *J Neurosci Methods*. 166 (1), 41–52. <https://doi.org/10.1016/j.jneumeth.2007.06.026>.

Sugden, R.J., Diamandis, P., 2023. Generalizable electroencephalographic classification of Parkinson’s disease using deep learning. *Inform Med Unlocked*. 42, 101352. <https://doi.org/10.1016/j.imu.2023.101352>.

Tao, J., Dan, Y., Zhou, D., 2024. Local domain generalization with low-rank constraint for EEG-based emotion recognition. *Front Neurosci*. 17, 1213099. <https://doi.org/10.3389/fnins.2023.1213099>.

Ung, H., Baldassano, S.N., Bink, H., Krieger, A.M., Williams, S., et al., 2017. Intracranial EEG fluctuates over months after implanting electrodes in human brain. *J Neural Eng*. 14 (5), 056011. <https://doi.org/10.1088/1741-2552/aa7f40>.

Wang, X., Chen, M., Shen, Y., Li, Y., Li, S., et al., 2024. A longitudinal electrophysiological and behavior dataset for PD rat in response to deep brain stimulation. *Sci Data*. 11 (1), 500. <https://doi.org/10.12751/g-node.lzvqb5>.

Wang, Y., Zhang, B., Tang, Y., 2024. DMMR: Cross-subject domain generalization for EEG-based emotion recognition via denoising mixed mutual reconstruction. In: Proceedings of the AAAI conference on artificial intelligence, Vol. 38, No. 1. pp. 628-636. <https://doi.org/10.1609/aaai.v38i1.27819>.

Weaver, F.M., Follett, K., Stern, M., Hur, K., Harris, C., et al., 2009. Bilateral deep brain stimulation vs best medical therapy for patients with advanced parkinson disease: A randomized controlled trial. *JAMA*. 301 (1), 63–73. <https://doi.org/10.1001/jama.2008.929>.

Woo, S., Zubair, M., Lim, S., Kim, D., 2024. Adversarial Training based Domain Adaptation for Cross-Subject Emotion Recognition. In: The Third Workshop on New Frontiers in Adversarial Machine Learning.

Yang, J., Zou, H., Zhou, Y., Xie, L., 2020. Towards stable and comprehensive domain alignment: Max-margin domain-adversarial training. arXiv preprint. <https://doi.org/10.48550/arXiv.2003.13249>.

Śliwowski, M., Martin, M., Souloumiac, A., Blachart, P., Aksanova, T., 2023. Impact of dataset size and long-term ECoG-based BCI usage on deep learning decoders performance. *Front Hum Neurosci.* 17, 1111645. <https://doi.org/10.3389/fnhum.2023.1111645>.